Supplementary Information

Microwave-Hydrometallurgical Extraction of $Li_4Ti_5O_{12}$, $LiFePO_4$ from Ilmenite: Effect of PPy-Br$_2$ Derived C-Coating with N, Br and Nb^{5+} Co-Doping on Electrodes for High-Rate Energy Storage Performance

T. Bonnisa Magdaline and A.Vadivel Murugan*

Advanced Functional Nanostructred Materials Laboratory, Centre for Nanoscience and Technology, Madanjeet School of Green Energy Technologies, Pondicherry University (A Central University), Dr. R. V. Nagar, Kalapet, Puducherry 605014, India.

*Email:avmrajeshwar@gmail.com; avmurugan.nst@pondiuni.edu.in
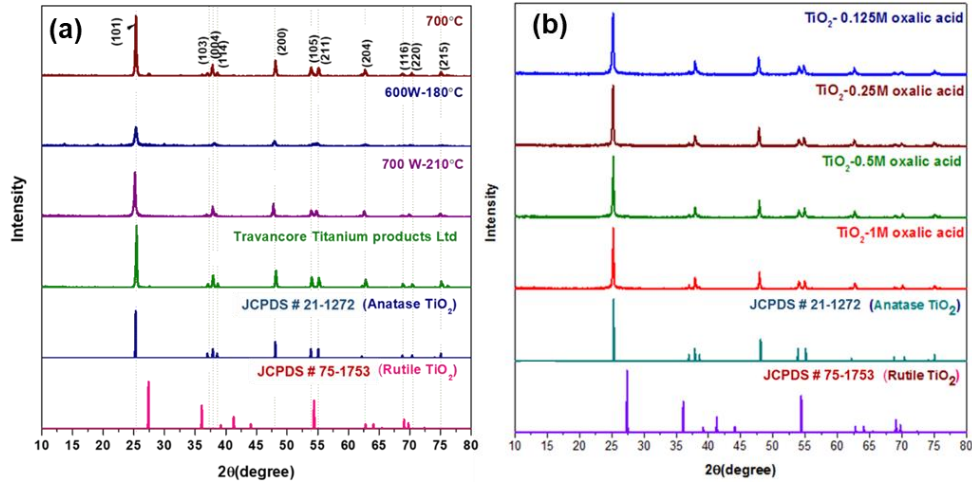
Tel: 91-413-2654975

Figure S1. (a) XRD analysis of TiO_2 anatase formation from $TiOSO_4$ by MW-HT method and (b) TiO_2 anatase optimization by varying the molar ratio of oxalic acid.

Figure S1a shows the XRD analysis of TiO_2 extracted from $TiOSO_4$ (ilmenite) by MW-HT process. The optimization was carried out for TiO_2 extraction (from $TiOSO_4$) by varying the reaction temperature and it was observed that the product formation was initiated at 180 °C which matches with the calcinated sample. **Figure S1b** shows the XRD analysis of TiO_2 extracted process by varying the concentration of oxalic acid and it was observed that pure phase TiO_2 was formed with the lowest concentration of (0.125M) oxalic acid which matches well along with the JCPDS card No 21-1272 with tetragonal crystal system of TiO_2 anatase.
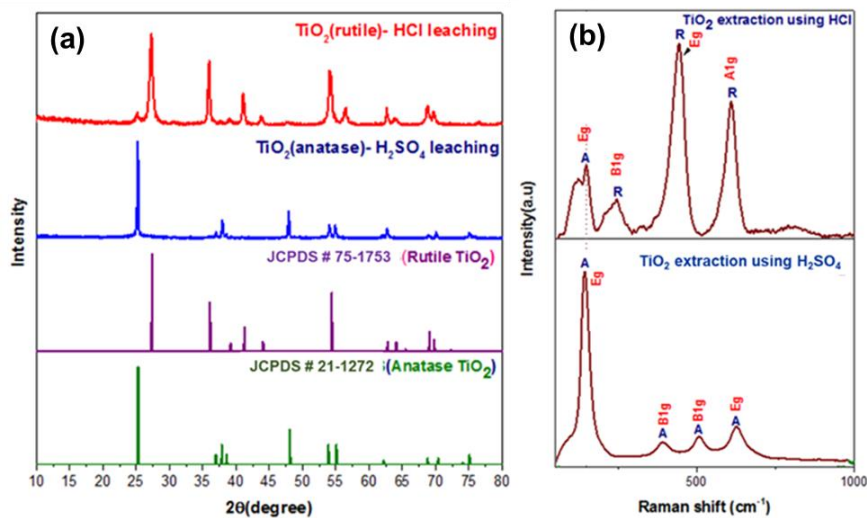

Figure S2. (a) XRD analysis of TiO_2 by HCl and H_2SO_4 leaching process and (b) Raman analysis.

Figure S2a shows the XRD analysis of TiO_2 extracted from ilmenite by HCl and H_2SO_4 leaching process. The TiO_2 extracted from ilmenite by HCl process exhibits rutile phase of

TiO$_2$ and by H$_2$SO$_4$ leaching process it forms anatase phase. The Raman analysis in **Figure S2b** was correlated with the XRD data where the Raman spectrum of the TiO$_2$ peaks centered at centered at 152 cm^1 (E$_g$), 402 cm^{-1} (B$_{1g}$), 510 cm^{-1} (A$_{1g}$) and 641 cm^{-1} (E$_g$) were attributed to the anatase phase. The peaks at at 249 cm^{-1} (B$_{1g}$), 445 cm^{-1} (E$_g$) and 611 cm^{-1} (A$_{1g}$) was attributed to the rutile phase of TiO$_2$.

Table S1. Literature comparison between the reaction time, temperature, phases and cycle life of dual-phase LTO-RTO with our work.

No.	Phases	Reaction time and temperature Reaction method and post modification	Doping and coating	Discharge capacity at 1C rate (mAhg^{-1})	Cycle number	References
1	LTO, RTO	Hydrothermal reaction 180 °C- 36 h, Calcination (Ar atmosphere)	C	130	200	Wang et al.[1]
2	LTO, RTO	Autoclave 130 °C- 18 h; Calcination 500 °C- 3 h	-	195	200	Zhanga et al.[2]
3	LTO	Ball milling 850 °C- 24 h; Calcination 800 °C (Ar)- 12 h;	Nb	120	-	Kim et al.[3]
4	LTO	Sol gel 60 °C- 3 h; Calcination 800 °C- 10 h	Cr	155	1000	Zou et al.[4]
5	LTO	Spray drying 900 °C- 20 h; Ball milling; Refluxing 120 °C- 48 h; Calcination 600 °C (Ar)- 4 h	N doped C	174	100	Long et al.1[5]
6	LTO	Autoclave 180 °C-18 h; Calcination 600 °C- 3 h	PEDOT	170	100	Wang et al.[6]
7	LTO, RTO	Autoclave 180 °C- 6 h; Calcination 800 °C (N$_2$)- 2 h	-	150	60	Hwang et al.[7]
8	LTO	Ball milling; Calcination 800 °C- 4 h	Cu	150	200	Lin et al.[8]
9	LTO	Ball milling (300 rpm)- 4 h; Calcination 350 °C- 4 h; 850 °C- 12 h	V, C	169	20	Yang et al.[9]
10	LTO, Li$_2$TiO$_3$	Reverse microemulsion process 500 °C - 2 h; 700 °C - 6 h (N$_2$)	C, N, Br	172	500	Li et al.[10]
11	LTO, RTO	MW-SS 800 °C- 30 min (Ar/H$_2$)	Nb, N, C, Br	169	500	**This work**

Table S2. Literature Comparison between the reaction time, temperature, morphology and cyclability of LiFePO$_4$ with our work.

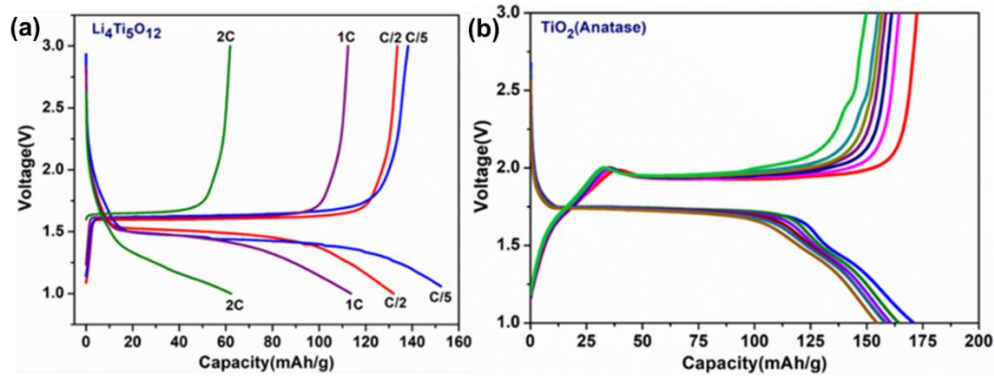| No.	Reaction time and temperature Reaction methods and post modification	Doping and coating	Morphology	Discharge capacity at 1C rate (mAhg^{-1})	Cycle number	References
1	Microwave solvothermal 300 °C- 5 min	C	Nanorods	157	50	Murugan *et al.*[11]
2	Calcination 350 °C- 4 h (N$_2$); 750 °C- 6 h	Nb, C	Agglomerated particles	105	20	Zhang *et al.*[12]
3	CHFS process 335 °C; Calcination 700 °C (Ar)- 3 h	Nb, C	Semi-spherical and rhombic-morphology particles	158	200	Johnson *et al.*[13]
4	Sol-gel 40 °C-1 h; Calcination 800 °C	C	Micro porous structure	104	35	Hasegawa *et al.*[14]
5	Refluxing 240 °C- 14 h; Calcination 600 °C- 10 h (Ar/N$_2$)	CNT, Graphene	Lamellar structure	127	100	Lu *et al.*[15]
6	Solvothermal reaction by autoclave 180 °C-10 h; Calcination 700 °C- 8 h (Ar)	N doped C, GO	Aggregated nanoparticles	146	500	Oh *et al.*[16]
7	Dual templating method 140 °C- 24 h; Calcination 600 °C (N$_2$) - 24 h	C	Hierarchical porous morphology	123	110	Vu *et al.*[17]
8	MW-HT reaction 220 °C - 25 min; MW-SS reaction 700 °C- 30 min (Ar/H$_2$)	Nb, N, C, Br	Nanorods	157	500	**This work**

Figure S5 (a) Electrochemical performance of pure phase of $Li_4Ti_5O_{12}$ and (b) charge-discharge profile TiO_2 anatase.

Figure S5a shows the charge discharge profile of $Li_4Ti_5O_{12}$ cycled with a voltage window of 1- 3 V *vs* Li^+/Li at different C rate from C/5, C/2, 1C and 2C where it shows a discharge capacity of 165 $mAhg^{-1}$ at C/5 rate, 138, 119 and 65 $mAhg^{-1}$ at C/2, 1C and 2C rate.

Table S3: Rietveld refinement factors of LTO-RTO, LTNO-RTO, LFP and LFNP

Samples	Chemical formula	Formula weight	Z	Rietveld refinement factors	
				χ^2	R(Bragg)
LTO-RTO	$Li_{1.33} Ti_{1.67}O_4$	153.06	8	1.895	15.77
LTNO-RTO	$Li_{1.33}Ti_{1.62}Nb_{0.05}O_4$	153.60	8	1.394	15.05
LFP	$LiFePO_4$	157.76	4	1.141	17.33
LFNP	$LiFe_{0.99}Nb_{0.01}PO_4$	157.79	4	1.213	17.85

Rigaku Ultima IV X-ray diffractometer with Cu Ka radiation (l = 1.54 Å) at 40 kV and 30 mA were scanned at diffraction angles from 10˚ to 80˚ with step size of 0.02°/second to carry out the XRD analysis which is compared with standard ICDD (International Centre for Diffraction Data). Rietveld analyses were carried out by using GSAS software and CIF files of LFP, LFNP, LTO-RTO and LTNO-RTO. The R-factors are defined as given below:

$$R_p = \frac{\sum |I_o - I_c|}{\sum I_o}$$...(1)

$$R_{wp} = \sqrt{\frac{M_p}{\sum wI_o^2}}$$ ....(2)

The band gap (Eg) of the material was calculated by the equation given below where h denotes Plank's constant, α is absorption coefficient, n is type of optical transition, ν is light frequency whereas A is proportionality constant. The Eg (band gap) values of LTO-RTO, LTNO-RTO, NBC-LTNO-RTO, LFP, PFNP and NBC-LFNP were obtained from Tauc plot.

$$\alpha h\nu = A(h\nu - Eg)^{n/2} \ldots\ldots\ldots\ldots\ldots\ldots\ldots\ldots\ldots\ldots\ldots\ldots\ldots\ldots\ldots\ldots\ldots\ldots\ldots\ldots S1$$
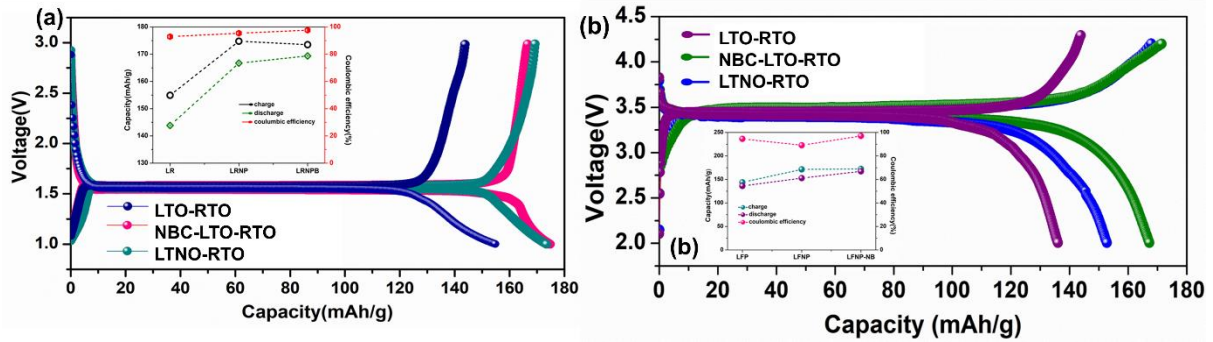

Figure S6. (a) Charge-discharge voltage profile of LFP, LFNP, NBC-LFNP cycled between voltage window of 2.0 V – 4.2 V *vs* Li$^+$/Li (b) LTO-RTO, LTNO-RTO and NBC-LTNO-RTO at C/5 rate cycled between potential range of 1.0 V – 3.0 V *vs* Li$^+$/Li (sub graph coulombic efficiency for 1st cycle).

Table S4: Rate-capability of LTO-RTO, LTNO-RTO, NBC-LTNO-RTO, LFP, LFNP and NBC-LFNP

C rate	LTO-RTO (mAhg^{-1})	LTNO-RTO (mAhg^{-1})	NBC-LTNO-RTO (mAhg^{-1})	LFP (mAhg^{-1})	LFNP (mAhg^{-1})	NBC-LFNP (mAhg^{-1})
C/5	169	173	174	136	153	167
C/2	158	168	171	120	144	161
1C	155	165	169	119	140	157
2C	113	157	167	97	135	151
5C	98	156	164	91	129	148
10C	84	138	158	70	111	137
20C	73	126	148	65	101	126

Table S5: Literature comparison of various Ilmenite extraction process.

No.	Extraction method	Leaching agents	Extracted products	References
1	Pre-oxidation-700 °C- 6 h; Leaching 105 °C- 24 h	HCl	Iron oxide, titanium oxide (rutile)	Vásquez et al.[20]
2	Leaching process by refluxing 280 °C-10 h	KOH, oxalic acid	Iron oxide, titanium oxide (anatase)	Yuanbo et al.[21]
3	Pre-oxidation 1000 °C- 16 h; Microwave reduction	HCl	Iron oxide, titanium oxide	Kelly et al.[22]
4	Leaching process by refluxing 80 °C- 2 h	HCl	Iron oxide; titanium oxide	Baba et al.[23]
5	Leaching process by refluxing 95 °C- 2 h	HCl, H_2SO_4	Iron oxide; titanium oxide (pseudorutile, rutile)	Mehdilo et al.[24]
6	Microwave hydrometallurgical extraction (MW-HM) 180 °C- 35 min	KOH, H_2SO_4	β- FeOOH, titanium oxide (anatase)	**This work**

Furthermore, the lattice parameters for the samples $Li_4Ti_{5-x}Nb_xO_{12}/RTO$ (x=0, 0.01, 0.03, 0.05, 0.1) with cubic crystal system were calculated using the following equation

$$\frac{1}{d^2} = \frac{h^2+k^2+l^2}{a^2} \dots\dots\dots\dots\dots\dots\dots\dots\dots\dots\dots\dots\dots\dots\dots\dots\dots\dots.S2$$

The lattice parameters a for the samples $LiFe_{1-x}Nb_xPO_4$ (x = 0, 0.01, 0.03, 0.05, 0.1) with orthorhombic crystal system were calculated using the following equation

$$\frac{1}{d^2} = \frac{h^2}{a^2} + \frac{k^2}{b^2} + \frac{l^2}{c^2} \dots\dots\dots\dots\dots\dots\dots\dots\dots\dots\dots\dots\dots\dots\dots\dots\dots.S3$$

The inter planar distance 'd' were calculated using Bragg's $\lambda = 2d \sin \theta$
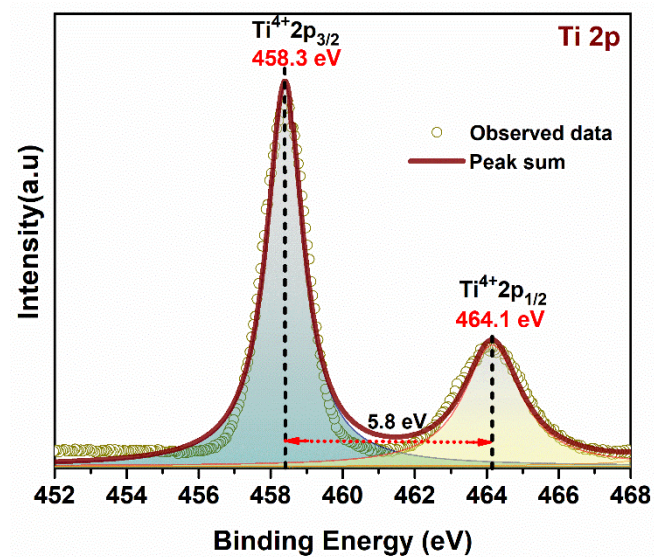
Figure S7. XPS spectra showing the Ti 2p spectra of LTO-RTO(x=0) revealing the of tetravalent oxidation states.

References:

1   P. Wang, G. Zhang, J. Cheng, Y. You, Y. K. Li, L. C. Ding, J. J. Gu, G. X. S. Zheng, C. F. Zhang and F. F. Cao, *ACS Appl. Mater. Interfaces,* 2017, **9**, 6138−6143.

2   Y. Zhanga, L. Huanga, Z. Zhoub, J. Wang, H. Liua and H. Wu, *Electrochimica Acta*, 2016, **195**, 124–133.

3   S. K. Kim, E. S. Kwon, T. H. Kim, J. Moon and J. Kim, *Ceramics International*, 2014, **40**, 8869-8874.

4   H. Zou, X. Liang, X. Feng and H. Xiang, *ACS Appl. Mater. Interfaces*, 2016, **8**, 21407−21416.

5   D. H. Long, M. G. Jeong,; Y. S. Lee, W. Choi, J. K. Lee, I. H. Oh and H. G. Jung, *ACS Appl. Mater. Interfaces*, 2015, **7**, 10250−10257.

6   Y. Q. Wang, L. Gu, Y. G. Guo, H. Li, X. Q. He, S. Tsukimoto, Y. Ikuhara and L. J. Wan, *J. Am. Chem. Soc.*, 2012, **134**, 7874−7879.

7   C. H. Hwang, H. Kim, I. Nam and J. H. Bang, *Nano Research*, 2019, **12**, 4, 897-904.

8   C. Lin, B. Ding, Y. Xin, F. Cheng, M. O. Lai, L. Lua and H. Zhou, *Journal of Power Sources*, 2014, 248.

9   C. C. Yang, H. C. Hu, S. J. Lin and W. C. Chien, *Journal of Power Sources,* 2014, **258**, 424-433.

10 Y. Li, Q. Chen, Q. Meng, S. Lei, C. Li, X. Li and J. Ma, *ACS Appl. Mater. Interfaces*, 2019, **11**, 25804−25816.

11 A. Vadivel, Murugan, T. Muraliganth and A. Manthiram, *Electrochemistry Communications*, 2008, **10**, 903–906.

12 A. Zhang, A. Li, J. Xia and Z. Shao, *Int. J. Electrochem. Sci.,* 2018, **13**, 5243-5252.

13 I. D. Johnson, E. Blagovidova, P. A. Dingwall, D. J. L. Brett, P. R. Shearing and J. A. Darr, *Journal of Power Sources*, 2016, **326**, 476-481.

14 G. Hasegawa, Y. Ishihara, K. Kanamori, K. Miyazaki, Y. Yamada, K. Nakanishi, T. Abe, *Chem. Mater.,* 2011, **23**, 5208−5216.

15 J. Lu, Y. Zhoun, T. Jiang, X. Tian, X. Tu and P. Wang, *Ceramics International,* 2016, **42**, 1281−1292.

16 J. Oh, J. Lee, Y. Jeon, S. Park, J. M. Kim, T. Hwang, Y. Piao, *ACS Sustainable Chem. Eng.* 2019, **7**, 306− 314.

17 A. Vu and A. Stein, *Chem. Mater.*, 2011, **23**, 3237–3245.

18 Q. Pan, F. Zheng, X. Ou, C. Yang, X.Xiong, Z. T. Tang, L. Zhao and M. Liu, *ACS Sustainable Chem. Eng.,* 2017, **5**, 6, 4739-4745.

19 X. Yan, D. Sun, Y. Wang, Z. Zhang, W. Yan, J. Jiang, F. Ma, J. Liu, Y. Jin and Kanamura, *ACS Sustainable Chem. Eng.*, 2017, **5**, 6, 4637-4644.

20 R. Vásquez and A. Molina, *Metal*, 2008, **5**, 13-15.

21 W. Yuanbo, Q. I. Tao, C. Jinglong, Z. Wei, *Rare Metals*, 2010, **29**, 9-15.

22 R. M. Kelly and N. A. Rowson, *Minerals Engineering,* 1995, **8**, 11, 1427-1438.

23 A. A. Baba, F. A. Adekola, O. A. Arodola, L. Ibrahim, R. B. Bale, M. K. Ghosh, A. R. Sheik, *Metall. Mater. Eng.*, 2012, **18**, 1, 67-78.

24 A. Mehdilo and M. Irannajad, *Miner. Process.,* 2012*,* **48**, 2, 425−439.